Escola Tècnica Superior d'Enginyeries Industrial i Aeronàutica de Terrassa

UNIVERSITAT POLITÈCNICA DE CATALUNYA

Study for the development of a computational model for the analysis of hybrid beams made of concrete and composites

Degree in Aerospace Vehicles Engineering

-ANNEX A: Evolution of the model-

AUTHOR: Ferran de la Fuente Pi

DIRECTOR: Lluis Gil Espert

CO-DIRECTOR: Catalin Andrei Neagoe

DELIVERY DATE: 29/05/2015

Contents

Figure Summary

Table Summary

Equation Summary

1. Complete interaction between concrete and GFRP

1.1. Linear simulations

First of all, an initial simulation with linear material properties and bonded contact between concrete and GFRP was simulated. The results of this simulations should match the experimental results at the initial part of the load-midspan deflection curve.

This can be observed in Figure 1 and Figure 2, which show the results for M2-HB1 and M2-HB3 tests.

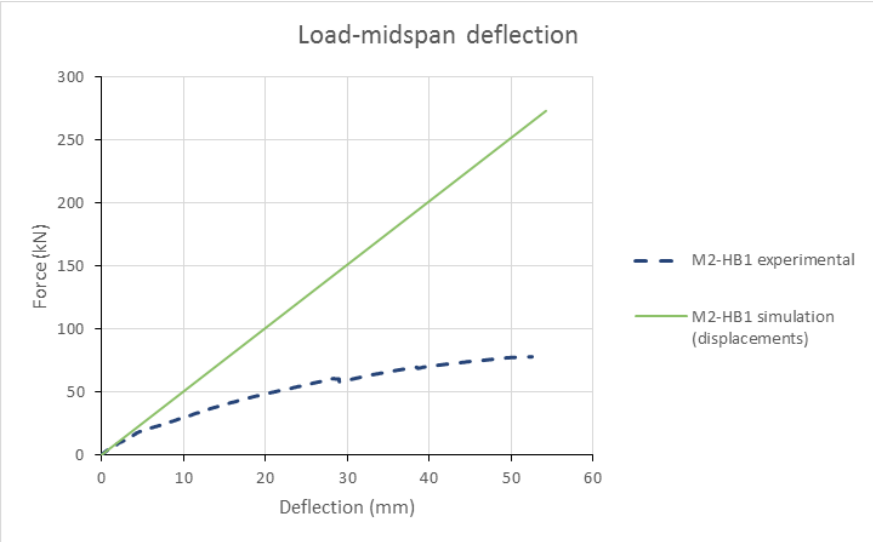

Figure 1. Load-midspan deflection results of the linear simulation for M2-HB1

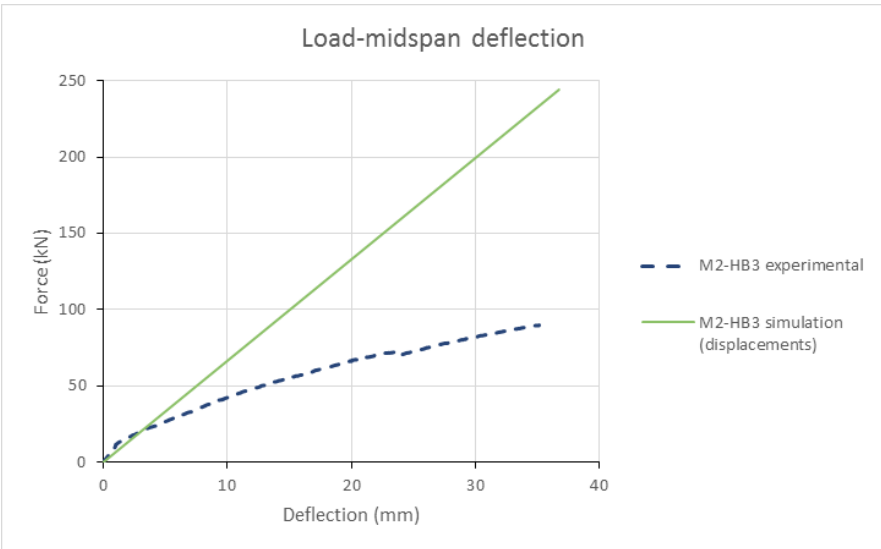

Figure 2. Load-midspan deflection results of the linear simulation for M2-HB3

1.2. Non-linear simulations

After the first initial linear simulations, the model is tested introducing the non-linear properties of concrete, but only considering compression properties. The obtained results are presented in

the charts below for all the tests, compared with the available experimental data and linear simulations.

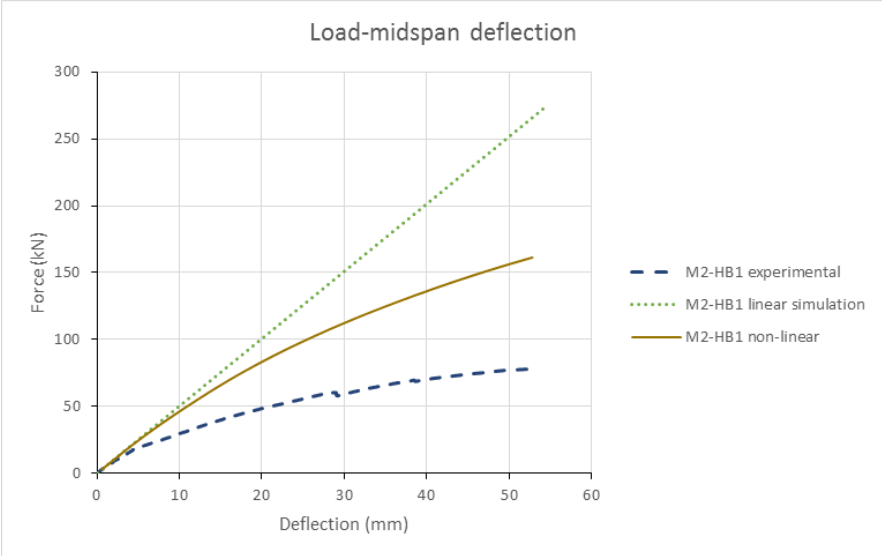

Figure 3. Load-midspan deflection comparative between experimental data, linear and non-linear simulation for M2-HB1 test

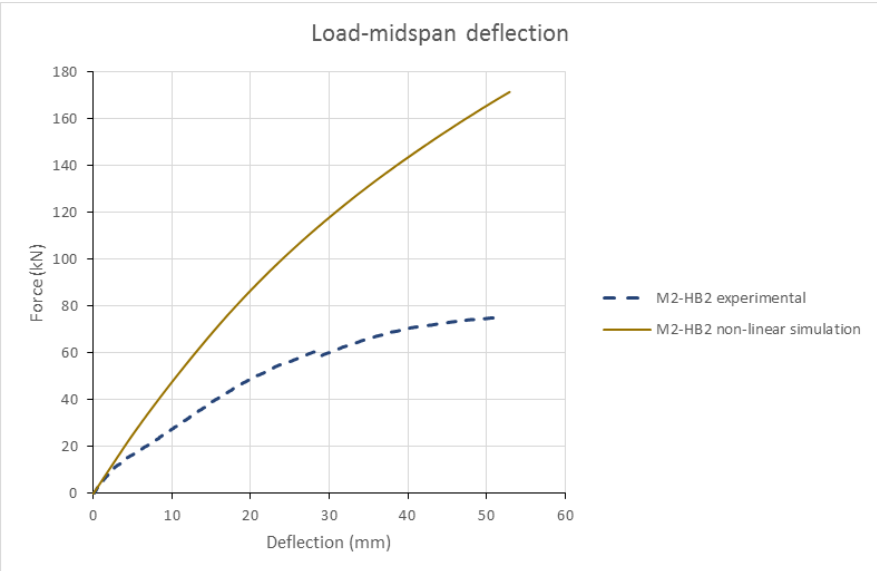

Figure 4. Load-midspan deflection comparative between experimental data and non-linear simulation for M2-HB2 test

It can be observed that the model is now more similar to reality after a plasticity model has been introduced. The results tend to become more similar to the observed behaviour in the experiments performed at LITEM. Moreover, this tendency will be increased when partial interaction effect are introduced in the model.

Additionally, Figure 5 and Figure 6 present the results for tests M2-HB3 and M2-HB4, confirming the tendency previously mentioned.

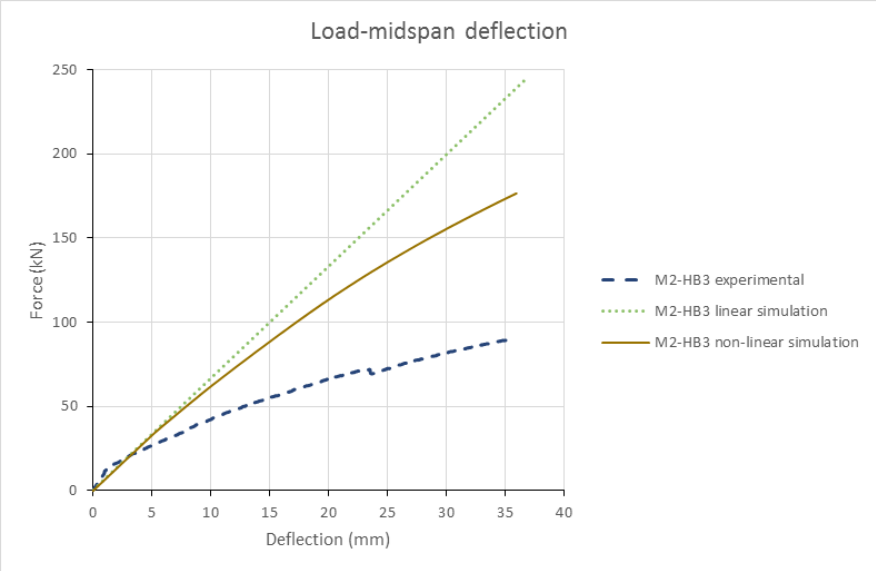

Figure 5. Load-midspan deflection comparative between experimental data, linear and non-linear simulation for M2-HB3 test

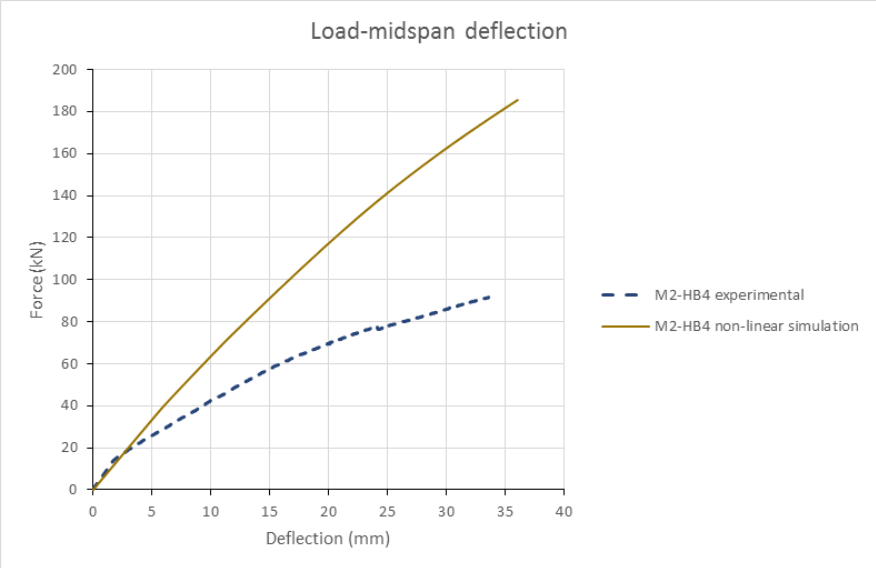

Figure 6. Load-midspan deflection comparative between experimental data and non-linear simulation for M2-HB4 test

However, non-linear effects can affect the convergence of the model and be problematic. In order to detect possible convergence issues, the force convergence chart for M2-HB1 simulation is presented below.

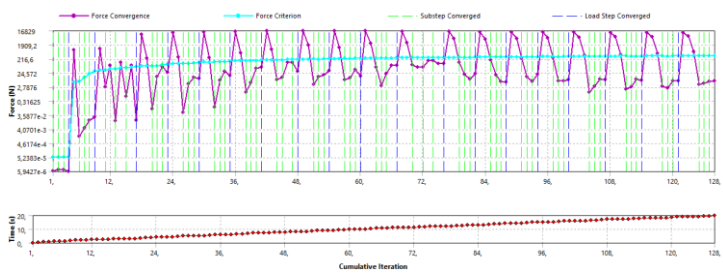

Figure 7. Force convergence chart for M2-HB1 non-linear simulation

This chart shows the force residual (purple line) versus the convergence criteria (blue line). As can be observed, no bisections have occurred, and every step converges with few iterations, so the solver settings seem correct to deal with future simulations.

Force convergence charts for the other three simulations have not been included because they are very similar to the presented one.

2. Partial interaction between concrete and GFRP

2.1. Non-linear simulations

2.1.1. Modelling the connections with springs

Spring elements are a type of connection element which restricts the displacement between two surfaces by means of a longitudinal stiffness. In a first approach, a more complex model of the beam, including the holes for the bolts have been used, as Figure 8 shows.

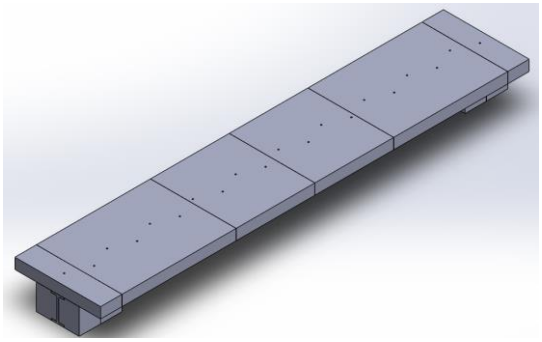

Figure 8. 3D geometry with holes for the bolts

Springs have been configured in order to link the inner surfaces of the holes of both parts of the beam. Using this more complex geometry, contacts, springs and solver configuration have been tested and optimized. After this, the simplification of the model was analysed, basically by considering how to include the springs without the presence of the holes.

2.1.1.1. Contact configuration

Contact takes place when two surfaces touch each other such that they become mutually tangent. The hybrid beam has two parts which are in contact. In order to define the type of contact which suits the most, the different possibilities offered by ANSYS are studied. Knowing the requirements of the connectors (only displacement in tangential direction), a no separation formulation would seem the better choice. However, the frictionless formulation is also taken into account.

The following chart present the results for both formulations using the first model with springs, discussed in the previous section.

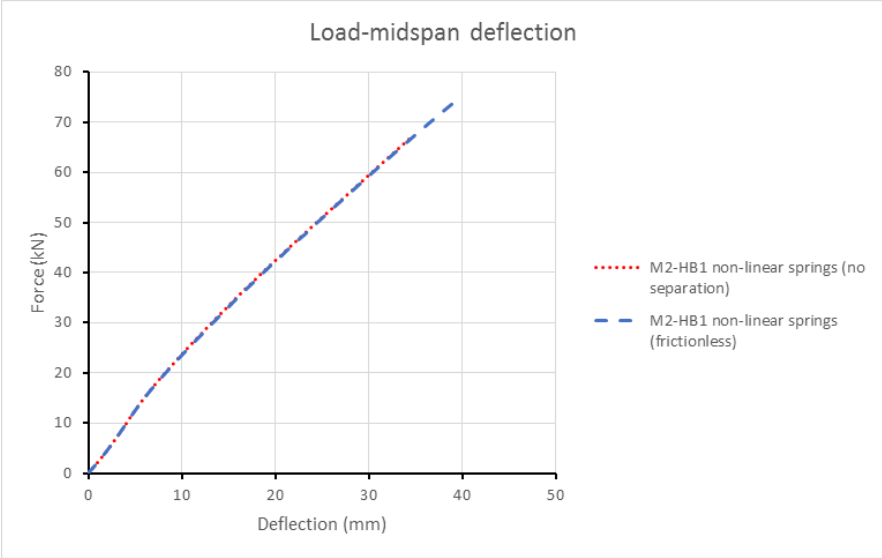

Figure 9. Load-midspan deflection results of the first model with springs using no separation and frictionless contact formulations

As the comparative chart shows, the results are coincident, so both formulations can be used. However, convergence is easier using a frictionless formulation. The main reason for that is the no separation formulation is forcing the model. In reality, the separation between GFRP and concrete is negligible, so it can be considered to be zero. However, in the simulation, if using the no separation formulation, these small separations are not allowed, and it makes the convergence more difficult.

Finally, and having tested that there is no difference between both, the frictionless formulation is used for all the models.

2.1.1.2. Spring configuration

First of all, the springs were introduced in the model by linking the inner surfaces as previously said. The result is presented in Figure 10. However, the desired effect of the spring connectors is shown in Figure 11. The problem with this first configuration come when a first simulation is made.

Because of the length of the spring (in this case is 29mm), the simulated shear stiffness of the spring is much lower than the real one, because small displacements along the longitudinal axis mean negligible increments of the spring's length. The results obtained from the simulation are presented in Figure 12.

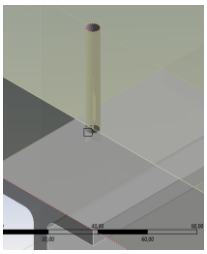

Figure 10. Detailed view of a spring connector (first model)

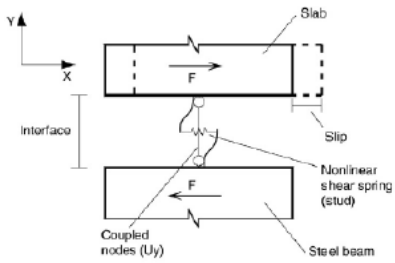

Figure 11. Desired effect of connectors

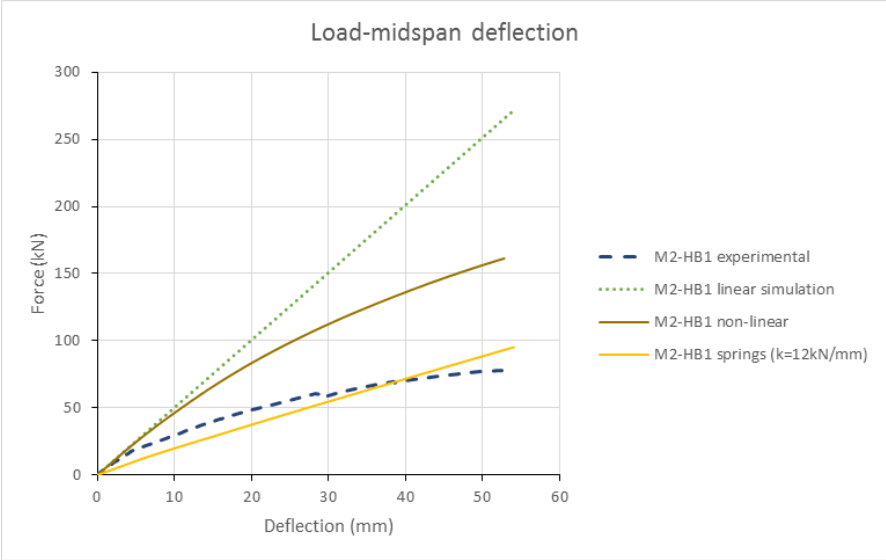

Figure 12. Load-midspan deflection chart for the first model with springs

The solution in order to increase the accuracy of the model is to reduce the spring's length. This new model is presented in Figure 13 and Figure 14. Using a shorter spring, the rigidity of the beam should approach more to reality than the initial simulation.

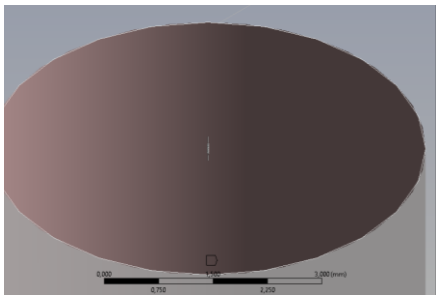

Figure 13. Detailed view of a spring connector (second model)

Definition	
Type	Longitudinal
Spring Behavior	Both
Longitudinal Stiffness	12000 N/mm
Longitudinal Damping	0, N·s/mm
Preload	None
Suppressed	No
Spring Length	0,4 mm

Figure 14. Main properties of the springs in the second model

The tendency of the model to become similar to reality if the length of the spring tends to zero is shown in the following chart.

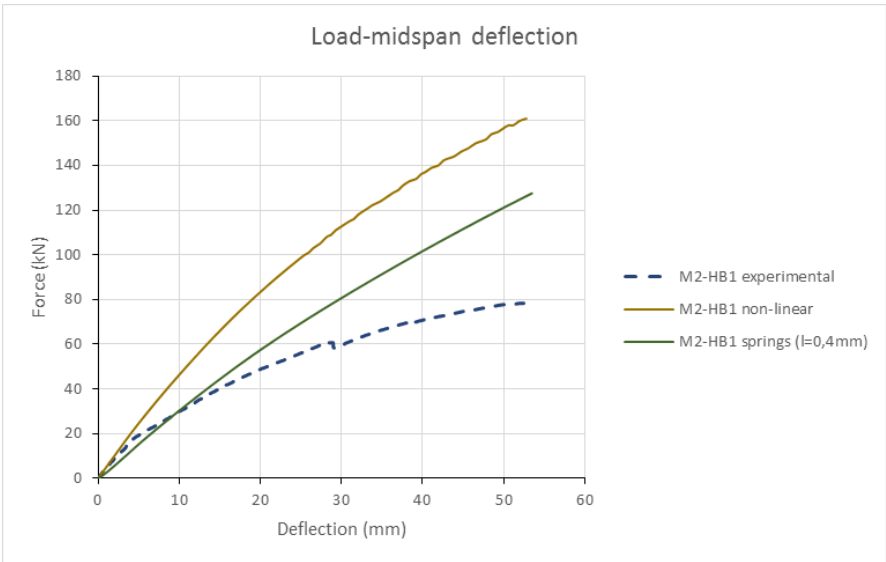

Figure 15. Load-midspan deflection chart for the second model with shorter springs

On the one hand, the results are much more similar to reality, because of a more consistent and real definition of the shear connectors. On the other hand, if the elongation of the central springs is analysed, the initial length of the spring is still significant (see Figure 16). The maximum elongation is 0,7mm, which is about the same order of magnitude than the length of the springs.

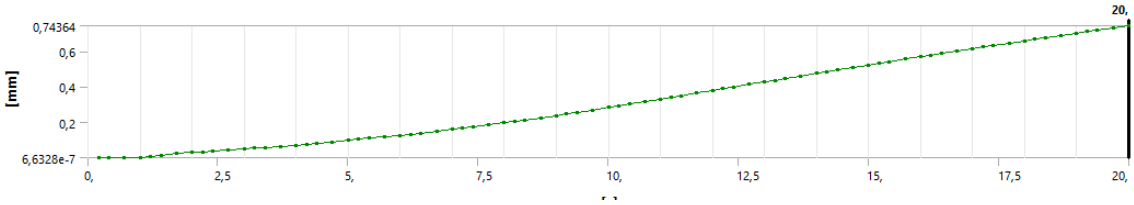

Figure 16. Elongation of the central springs

Furthermore, the problem of the length of the spring is affecting the results more for low values of spring elongation (the initial elongation is of the order of 0.01 mm). So as to obtain better results, the initial length of the spring is reduced four orders of magnitude (10^{-6} mm) to analyse differences. The obtained results are presented in Figure 17.

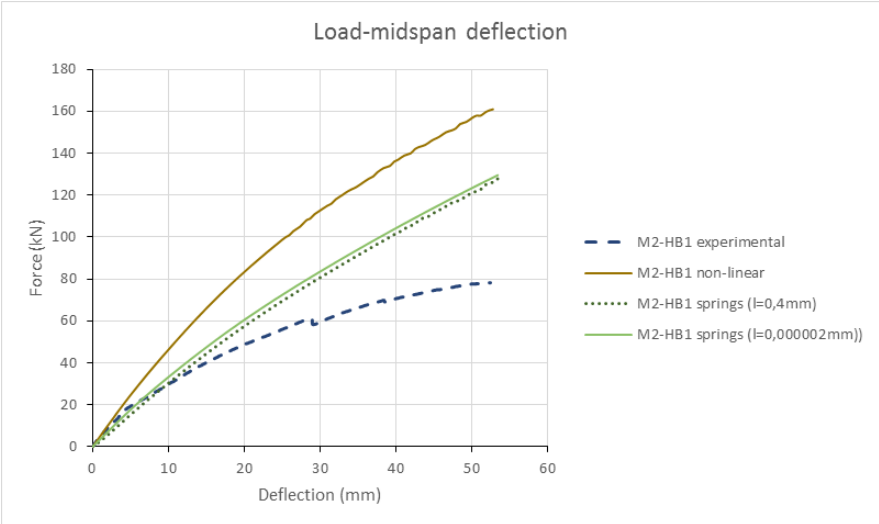

Figure 17. Effect of reducing the initial length of the springs

Figure 17 shows that the results are more accurate for the last simulation, with springs that have an initial length near zero.

Finally, the differences still present between the simulations and the experimental data are caused because of the plasticity of the connectors, which has not been included in the model. This effect will be analysed in the next section.

2.1.1.3. Non-linear behaviour of the connectors

In previous simulations the force capacity of the shear connectors has been considered to be unlimited, since a linear behaviour has been used. However, in reality, once the connections reach a limit, they can't withstand more loads. This means that a non-linear longitudinal stiffness of the springs must be defined. In order to do so, an elastic force limit is used according to an analytical solution of the connections from Eurocode 4 (European Standard 2004), this limit should be of 8kN of force for beams using concrete 1 and 9kN for beams using concrete 2.

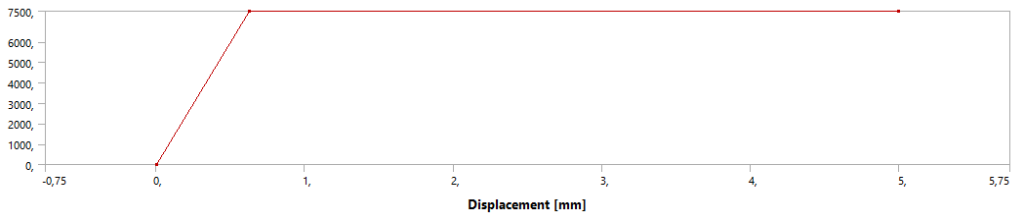

Figure 18. Example of the non-linear behaviour of the springs

However, another formulation for determining the maximum shear capacity of the connectors is used from FIB 2010 (International Federation for Structural Concrete 2010). Using this different formulation (see Equation 1), the value obtained for beams using concrete 1 (30MPa) is 11,95kN, and the value for concrete 2 (35MPa) is 12,84kN. Nevertheless, it is necessary to remember that the force limits calculated are from design codes for concrete and steel structures, so the real values for the present study should be lower, because the bolts are not welded to the GFRP part.

$$P_k = \left(5.3 - \frac{1.3}{\sqrt{n}}\right) \cdot A \cdot f_c^{0.35} \cdot f_t^{0.65} \cdot \left(\frac{E_c}{E_s}\right)^{0.4}$$

where:

A is the connector equivalent cross section;
f_c is the compressive strength of the concrete;
E_c is the modulus of elasticity of the concrete;
f_t is the ultimate tensile stress in steel;
E_s is the modulus of elasticity of steel.

Equation 1. Analytical formula for determining the maximum shear capacity of the bolted connection (International Federation for Structural Concrete 2010)

2.1.1.4. Final results using spring connectors

In the end, after the best configuration for the spring model is chosen, all the tests, each with its characteristics and loading scheme are simulated. The results are presented in the following charts, using non-linear springs for both shear connectors formulations (FIB 2010 and Eurocode 4). However, for the definitive model, the Eurocode 4 formulation is used for two reasons. First, the results with this approach are more accurate and similar to reality. Furthermore, Eurocode 4 is a mandatory code, while FIB 2010 is a design guide.

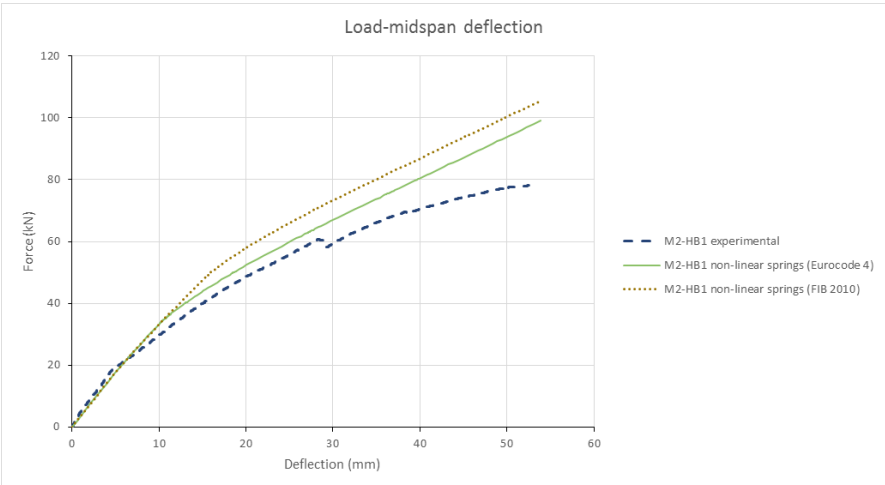

Figure 19. Load-midspan deflection results of the simulation for M2-HB1 test using the model with non-linear springs

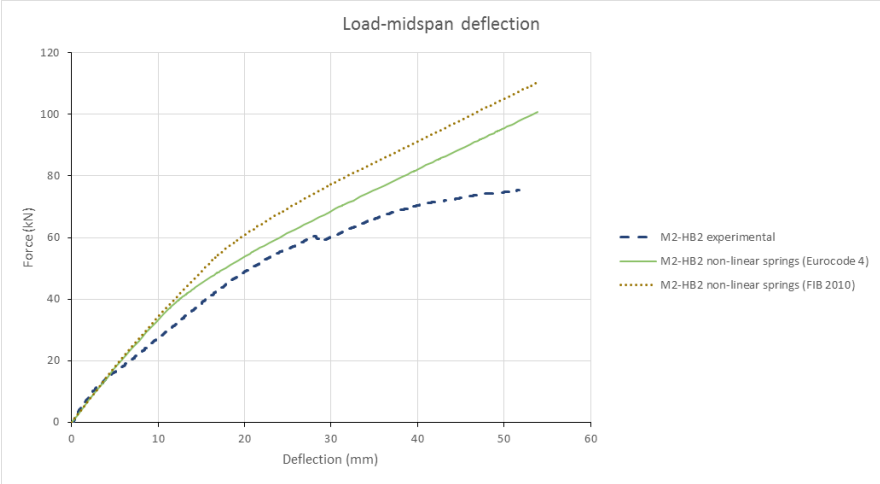

Figure 20. Load-midspan deflection results of the simulation for M2-HB2 test using the model with non-linear springs

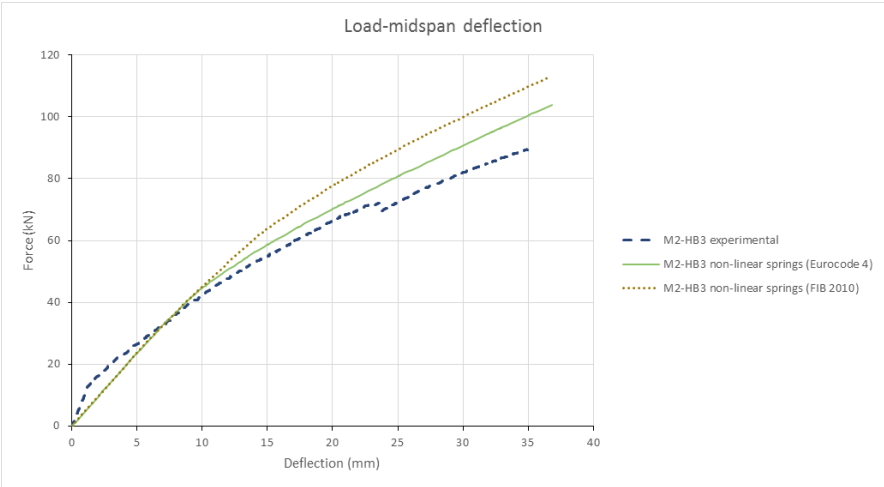

Figure 21. Load-midspan deflection results of the simulation for M2-HB3 test using the model with non-linear springs

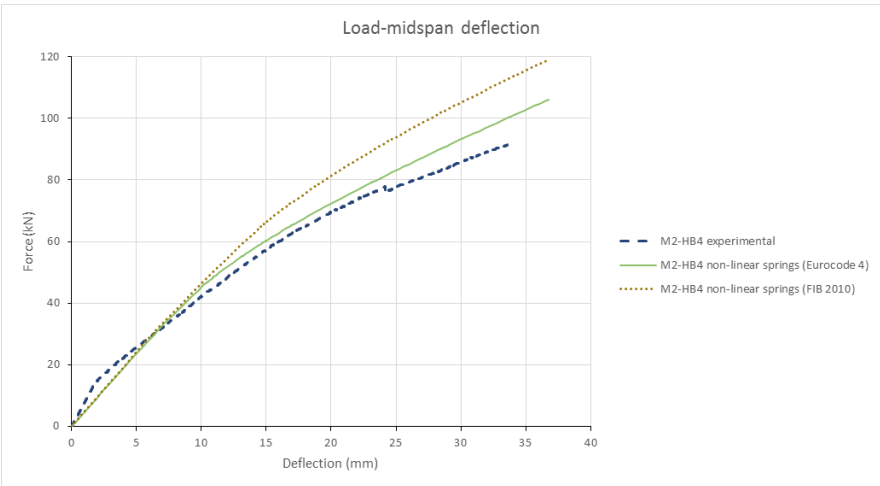

Figure 22. Load-midspan deflection results of the simulation for M2-HB4 test using the model with non-linear springs

2.1.2. Modelling the connections using beams

In this section, beam elements are used in order to simulate the stud connectors of the hybrid beam. A beam is a structural element that carries load primarily in axial and bending (flexure). Using the Beam feature, body-to-body or a body-to-ground connections can be established.

These beams, as in the previous section using springs, have been configured in order to link the inner surfaces of the holes of both parts of the beam. However, in this case, the length of the beam is set accordingly to the dimensions of the studs (35 mm). Moreover, these beam elements have a circular cross-section with a diameter of 6 mm.

2.1.2.1. Steel properties

First of all, it is necessary to define the steel of which studs are made. The used steel for the connections is an 8.8 quality steel. Its properties can be observed in Table 1.

Table 1. Material properties of steel

	Steel
Grade	8,8
Density (kg/dm3)	7,85
Tensile yield strength (MPa)	640
Tensile ultimate strength (MPa)	800
Young's modulus (GPa)	210
Poisson's ratio	0,3

Once the properties are known, it is necessary to introduce it in the model. In this case, as a first approach, a bilinear isotropic hardening (see Figure 23) has been chosen, with a perfect plastic behaviour.

Using this model for steel, results will be compared with the results using springs, and the better option will be chosen.

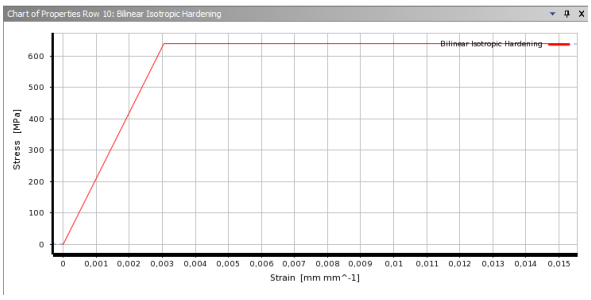

Figure 23. Bilinear isotropic hardening model for steel

2.1.2.2. Configuration of the beams

As previously said, the beams are configured by connecting the inner surfaces of the holes. The resulting configuration is shown in Figure 24.

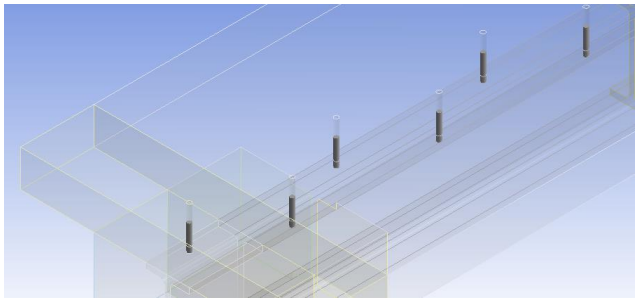

Figure 24. Detailed view of the beams in the model

As the figure shows, the beams have been introduced with the same diameter and length that the studs had. Furthermore, the configuration introduced in ANSYS Mechanical can be observed in Figure 25. In a first approach, the behaviour of the beams has been set to deformable.

Definition	
Material	Steel
Cross Section	Circular
Radius	3, mm
Suppressed	No
Scope	
Scope	Body-Body
Reference	
Scoping Method	Geometry Selection
Applied By	Remote Attachment
Scope	1 Face
Body	Cortar-Extruir1[2]
Coordinate System	Global Coordinate System
Reference X Coordinate	20, mm
Reference Y Coordinate	87, mm
Reference Z Coordinate	50, mm
Reference Location	Click to Change
Behavior	Deformable
Pinball Region	All
Mobile	
Scoping Method	Geometry Selection
Applied By	Remote Attachment
Scope	1 Face
Body	Cortar-Extruir1[8]
Coordinate System	Global Coordinate System
Mobile X Coordinate	20, mm
Mobile Y Coordinate	52, mm
Mobile Z Coordinate	50, mm
Mobile Location	Click to Change
Behavior	Deformable
Pinball Region	All

Figure 25. Configuration of one of the beams in the model

2.1.2.3. Contact configuration

The contact formulation used in this simulation using beams has been frictionless (see Figure 26), which as previously determined was the best suited option.

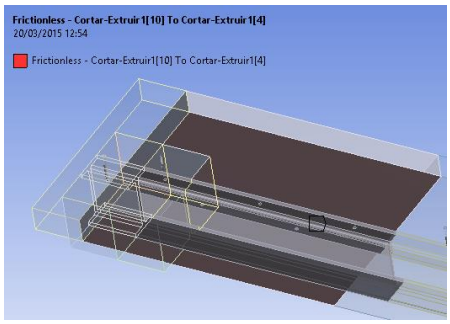

Figure 26. Frictionless contact formulation of the model

2.1.2.4. Solver configuration

The initial configuration for the solver was the one used in previous sections, which has been stable and robust by the moment. Figure 27 presents the force convergence chart for M2-HB1 simulation using beams (with rigid behaviour). It shows that this configuration is applicable in this case as well.

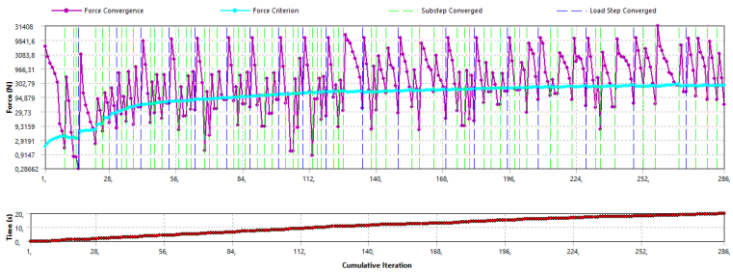

Figure 27. Force convergence chart for simulation M2-HB1 using beam connectors (rigid behaviour)

Nevertheless, for the second simulation, using a deformable behaviour for the beams, problems appear, needing the solver to do many bisections, and simulation finally fails to converge the last step (see Figure 28).

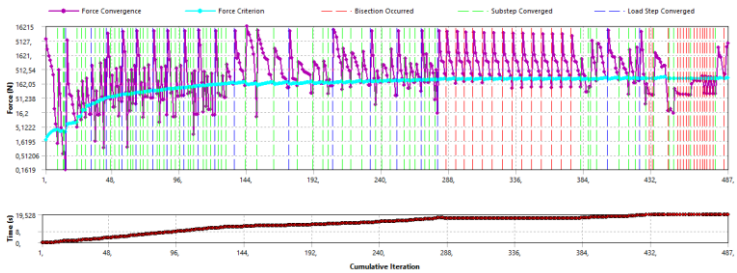

Figure 28. Force convergence chart for simulation M2-HB1 using beam connectors (deformable behaviour)

2.1.2.5. Final results using beam connectors

Finally, the simulations are executed in order to compare with spring connectors, and find out which configurations suits the most. The results for the four simulations are presented in the following charts.

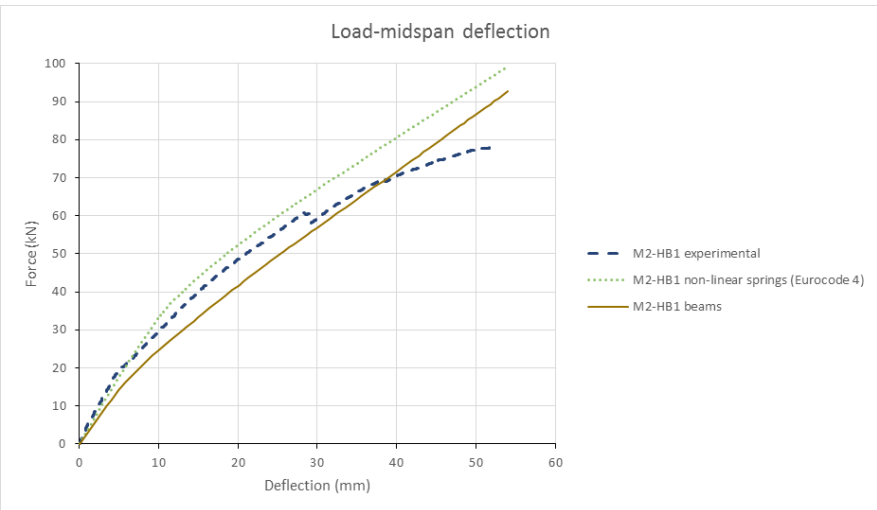

Figure 29. Load-midspan deflection chart of M2-HB1 simulation using beams

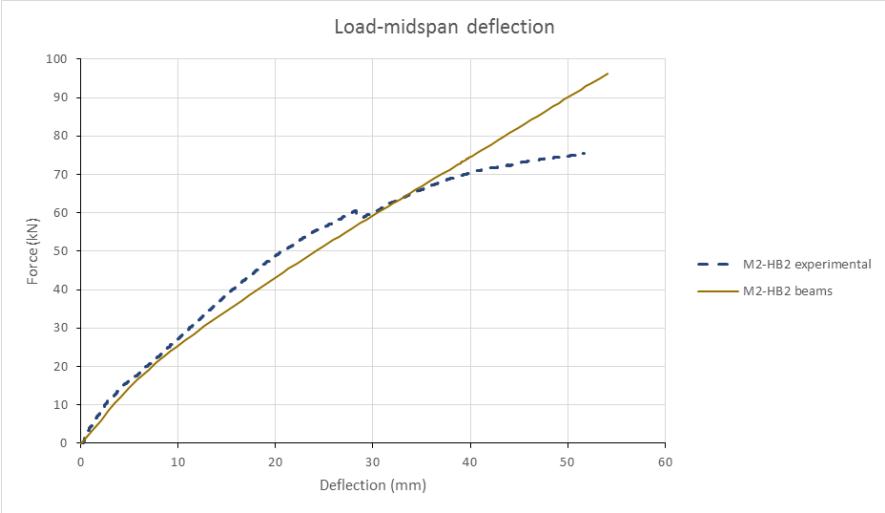

Figure 30. Load-midspan deflection chart of M2-HB2 simulation using beams

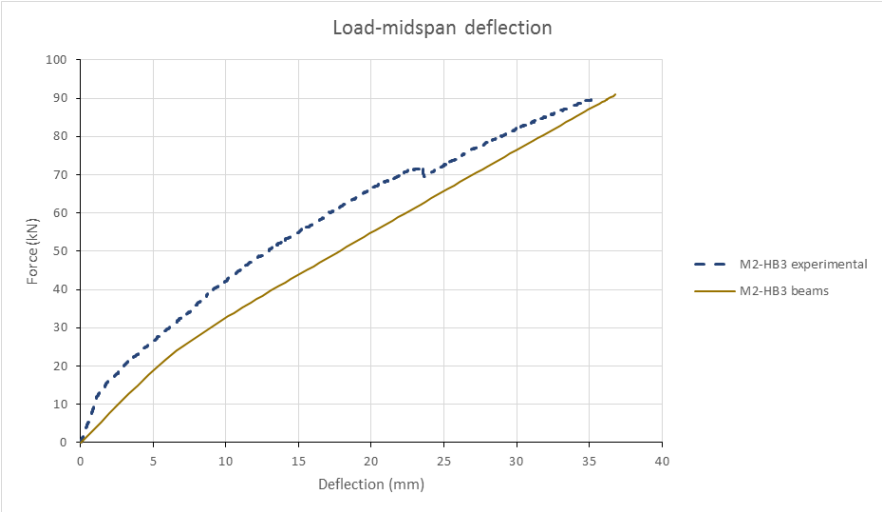

Figure 31. Load-midspan deflection chart of M2-HB3 simulation using beams

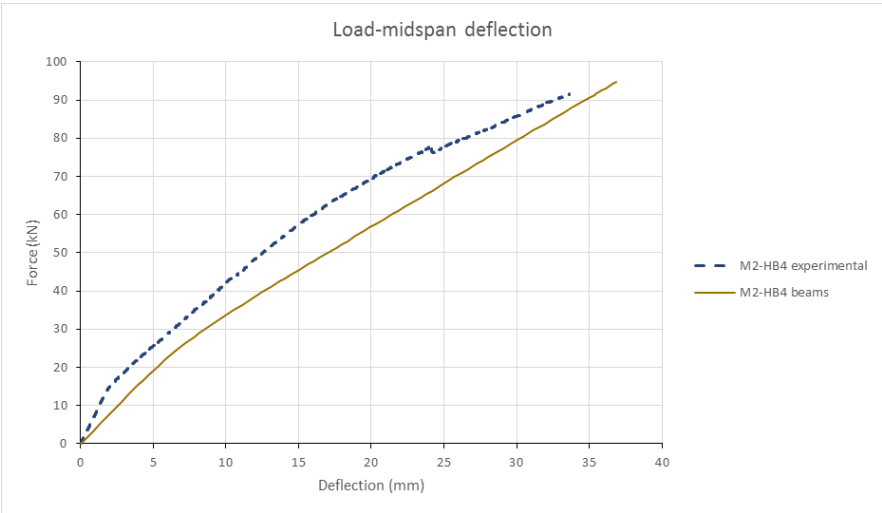

Figure 32. Load-midspan deflection chart of M2-HB4 simulation using beams

Compared to the previous simulations using springs, the simulations using beams are not fitting the load-midspan curve as well. The main reasons for that could be that the beam elements are not restricting enough the slip between GFRP and concrete, and this causes connections to have less shear stiffness, being a more conservative approach.

Furthermore, the model with springs is more accurate than the one with beams, so springs will be used in the definitive model, after its optimization.

2.1.3. Simplification of the model with springs

2.1.3.1. Model without holes

After the parameters of the simulations with springs are decided, simplifications for the model are studied. The aim of this simplifications is to eliminate the holes, so a hexahedral mesh with less elements can be used.

Initially, the possibility of not dividing the model, linking the surfaces with springs at different points (where the connectors are located) is studied. Figure 33 shows the configuration for one spring, and as previously said, the coordinates of the linked points can be observed for both reference and mobile bodies.

Graphics Properties	
Definition	
Type	Longitudinal
Spring Behavior	Both
Longitudinal Stiffness	12000 N/mm
Longitudinal Damping	0, N·s/mm
Preload	None
Suppressed	No
Spring Length	1,0021e-003 mm
Scope	
Scope	Body-Body
Reference	
Scoping Method	Geometry Selection
Applied By	Remote Attachment
Scope	1 Face
Body	Partir1[3]
Coordinate System	Global Coordinate System
Reference X Coordinate	20, mm
Reference Y Coordinate	60,001 mm
Reference Z Coordinate	1950, mm
Reference Location	Click to Change
Behavior	Rigid
Pinball Region	All
Mobile	
Scoping Method	Geometry Selection
Applied By	Remote Attachment
Scope	1 Face
Body	Partir1[13]
Coordinate System	Global Coordinate System
Mobile X Coordinate	20, mm
Mobile Y Coordinate	60, mm
Mobile Z Coordinate	1950, mm
Mobile Location	Click to Change
Behavior	Rigid
Pinball Region	All

Figure 33. Configuration for the first spring in the simplified model

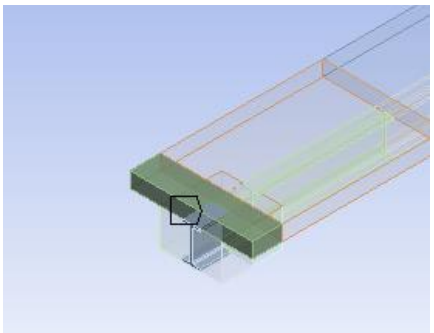

Figure 34. Detailed view of the spring configuration for the simplified model

However, the results of the simulation are completely unreal and it also has many convergence problems, being necessary for the solver to execute many bisections and being necessary more than 800 iterations to solve the model.

In a second attempt, the geometry is modified in order to have vertices where the springs have to be placed. The geometry is shown in Figure 35.

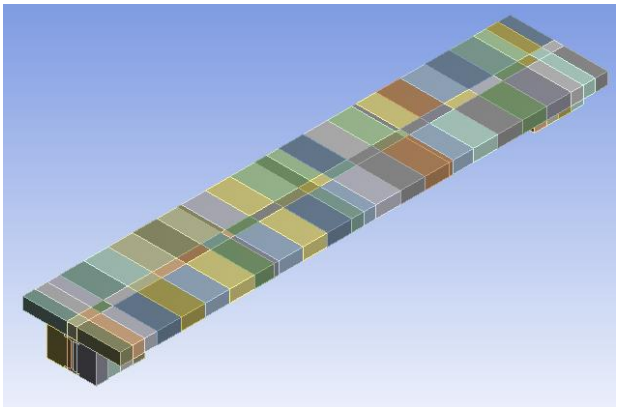

Figure 35. Geometry model with vertices at each connection point

As can be observed, this is a much more complex geometry model, with more than 200 bodies. However, problems appear when springs are intended to be applied on vertices, because ANSYS doesn't recognize the configuration (see Figure 36), so this simplification is also discarded.

Definition	
Type	Longitudinal
Spring Behavior	Both
Longitudinal Stiffness	12000 N/mm
Longitudinal Damping	0, N-s/mm
Preload	None
Suppressed	No
Spring Length	1,e-003 mm
Scope	
Scope	Body-Body
Reference	
Scoping Method	Geometry Selection
Applied By	Remote Attachment
Scope	1 Vertex
Body	Multiple
Coordinate System	Global Coordinate System
Reference X Coordinate	20, mm
Reference Y Coordinate	60,001 mm
Reference Z Coordinate	1950, mm
Behavior	Rigid
Pinball Region	All
Mobile	
Scoping Method	Geometry Selection
Applied By	Remote Attachment
Scope	1 Vertex
Body	Multiple
Coordinate System	Global Coordinate System
Mobile X Coordinate	20, mm
Mobile Y Coordinate	60, mm
Mobile Z Coordinate	1950, mm
Behavior	Rigid
Pinball Region	All

Figure 36. Configuration for the first spring in the simplified model with vertices at each connection point

2.1.3.2. Simplification using 2D elements

During this section, a possible reduction of the model complexity will be studied, using 2D elements instead of 3D elements, thereby reducing the CPU consumption.

2.1.3.2.1. Using 2D elements for concrete and GFRP with complete interaction

First of all, an initial geometry model using in all parts surface elements is generated. A view of this initial model is shown in Figure 37.

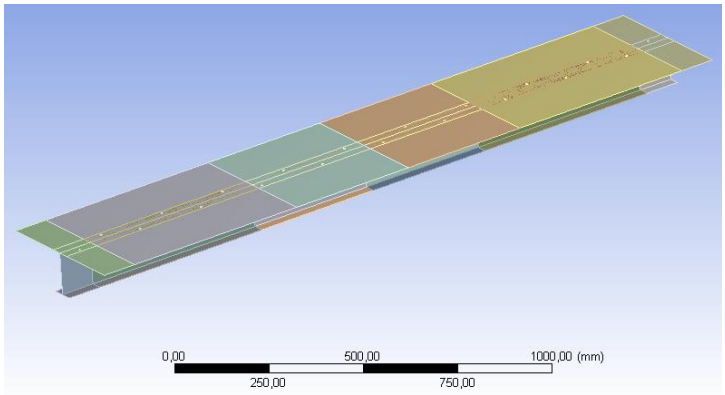

Figure 37. View of the model using 2D elements for concrete and GFRP

Moreover, Figure 38 shows the meshed model, once a thickness has been assigned to the shell elements. However, if a closer view of the model is observed (see Figure 39), differences between the model and the real hybrid beam can be appreciated.

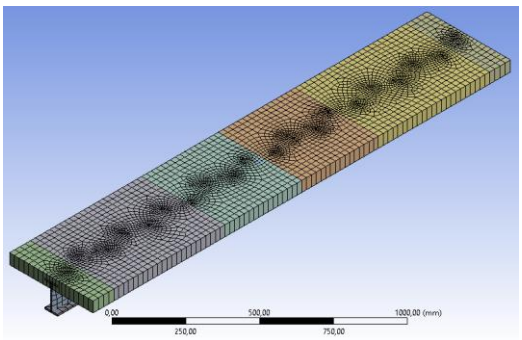

Figure 38. View of the meshed model using 2D elements for concrete and GFRP

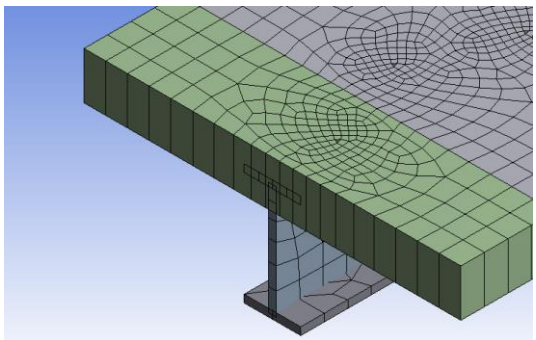

Figure 39. Detailed view of the meshed model using 2D elements for concrete and GFRP

These differences are caused because in ANSYS, 2D elements are defined by means of a mid-plane and a thickness. Despite this, the simulation is executed with a bonded contact formulation (complete interaction) in order to analyse the results.

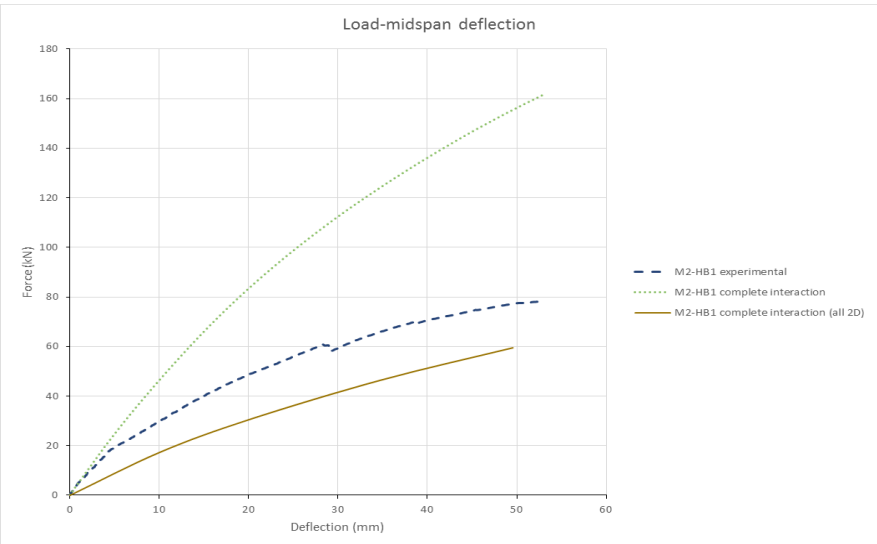

Figure 40. Load-midspan deflection comparative chart between simulations using 2D and 3D elements

Figure 40 shows the results for M2-HB1 simulation. As can be observed, this model is not able to simulate the behaviour of the hybrid beam, the simulated beam is much less rigid than the real one. This makes the results completely unreal. In an attempt to obtain better results, in the following section a different model is studied.

2.1.3.2.2. Using 2D elements for GFRP and 3D elements for concrete with complete interaction

In a second approach, a new geometry model (see Figure 41) using shell elements for GFRP part is generated. Using this new model, the same simulation from the previous section (which uses shell elements in all the model) is repeated, in order to observe differences. Furthermore, the meshed model is shown in Figure 42.

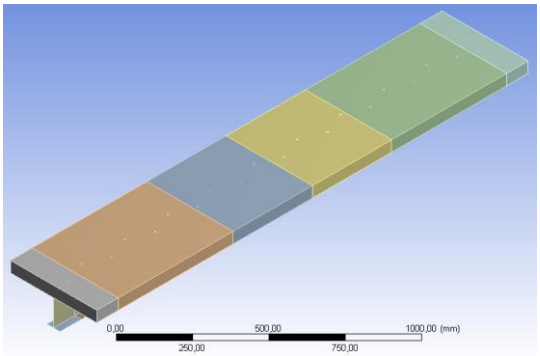

Figure 41. View of the model using 2D elements for GFRP

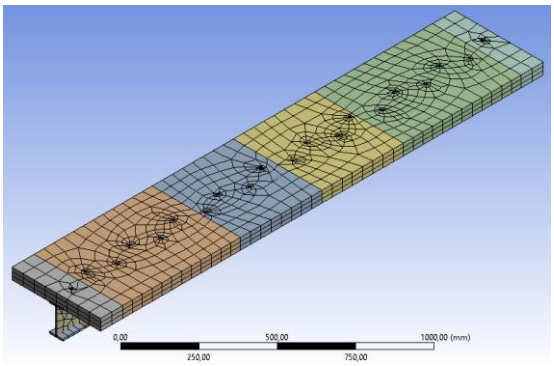

Figure 42. View of the meshed model using 2D elements for GFRP

Compared to the previous model, and observing a zoomed view of the actual meshed model (see Figure 43), it can be appreciated that this model is much more similar to the real one. However, first it is necessary to analyse the results from the simulation.

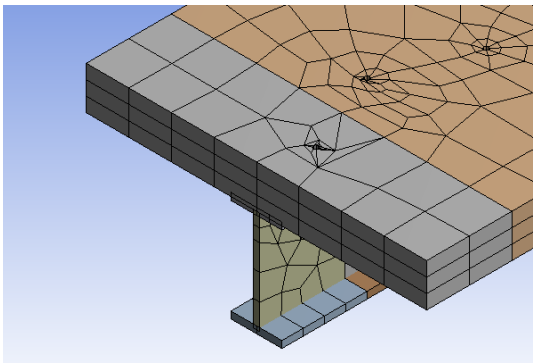

Figure 43. Detailed view of the meshed model using 2D elements for GFRP

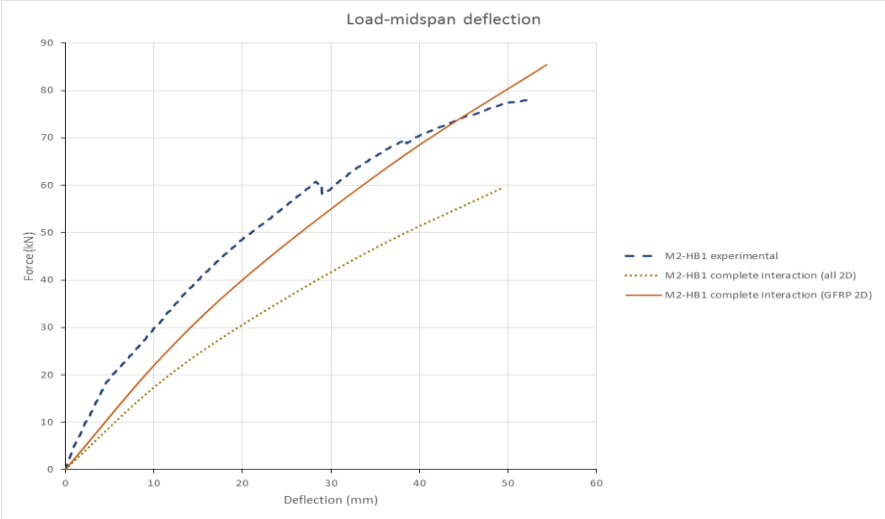

Figure 44. Load-midspan deflection comparative chart between simulations using 2D (only GFRP part) and 3D elements

Comparing to the initial 2D model, the results are significantly better. However, these results are still very poor compared to the simulations which use 3D elements. It seems like using the present configuration, these shell elements are not able to simulate completely the real behaviour of the GFRP column. Nevertheless, simulations including partial interaction of the components will be made in order to study its results as well in the section below.

2.1.3.2.3. Using 2D elements for GFRP and 3D elements for concrete with partial interaction

Finally, the second model using 2D elements is used for a new simulation, which includes spring elements in order to simulate the partial interaction. These springs have been configured as previously explained in this section, although in this case, the springs are attached between the inner surface of the holes (concrete part) and the circular edge of the holes (GFRP part) as Figure 45 shows.

Definition	
Type	Longitudinal
Spring Behavior	Both
Longitudinal Stiffness	Tabular Data
Longitudinal Damping	0, N-s/mm
Preload	None
Suppressed	No
Spring Length	1,0047e-004 mm
Scope	
Scope	Body-Body
Reference	
Scoping Method	Geometry Selection
Applied By	Remote Attachment
Scope	1 Face
Body	Solid
Coordinate System	Global Coordinate System
Reference X Coordinate	20, mm
Reference Y Coordinate	0, mm
Reference Z Coordinate	950, mm
Reference Location	Click to Change
Behavior	Rigid
Pinball Region	All
Mobile	
Scoping Method	Geometry Selection
Applied By	Remote Attachment
Scope	1 Edge
Body	Surface Body
Coordinate System	Global Coordinate System
Mobile X Coordinate	20, mm
Mobile Y Coordinate	-1,e-004 mm
Mobile Z Coordinate	950, mm
Mobile Location	Click to Change
Behavior	Rigid
Pinball Region	All

Figure 45. Configuration settings of one springs for the model using 2D elements for GFRP

Below, the results of the simulations for M2-HB1 test are presented in the comparative chart with the experimental results. This chart show that the results using shell elements are not corresponded with experimental results, so a good model should include 3D elements, which were the initially used and the ones which gave the best results.

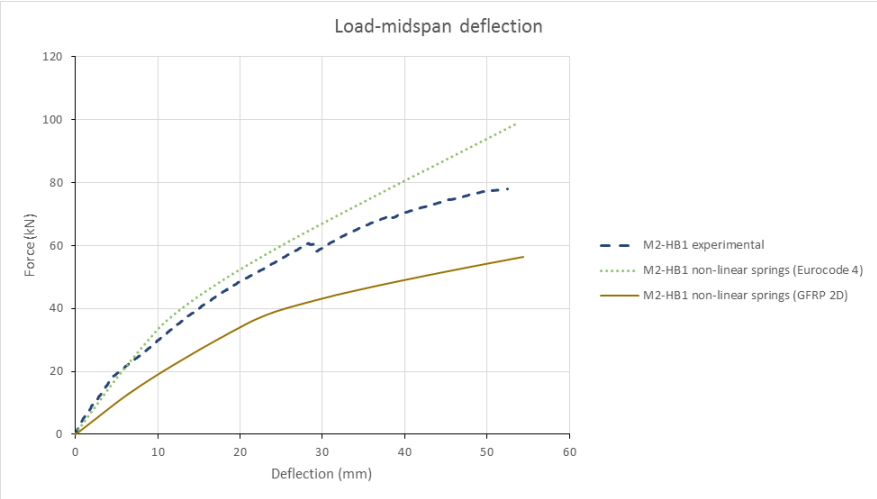

Figure 46. Load-midspan deflection results for M2-HB1 test using shell elements for GFRP and springs

2.1.3.3. Removing the concrete reinforcement of the supports

Finally, the effect of including the concrete reinforcement of the supports is analysed. In order to compare to the model used until this section, a new model without the reinforcement is used (see Figure 47).

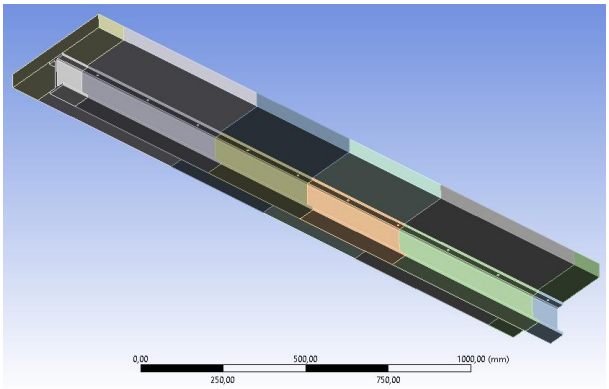

Figure 47. Geometry model without concrete reinforcement at the supports

Using this geometry model, a simulation using non-linear spring connectors is executed, and the results are presented in the chart below (see Figure 48).

The results start to become different for high values of load. This is why the concrete reinforcements will be maintained in the model, in order to develop a more accurate model. Moreover, the elapsed computing time for both simulations is very similar.

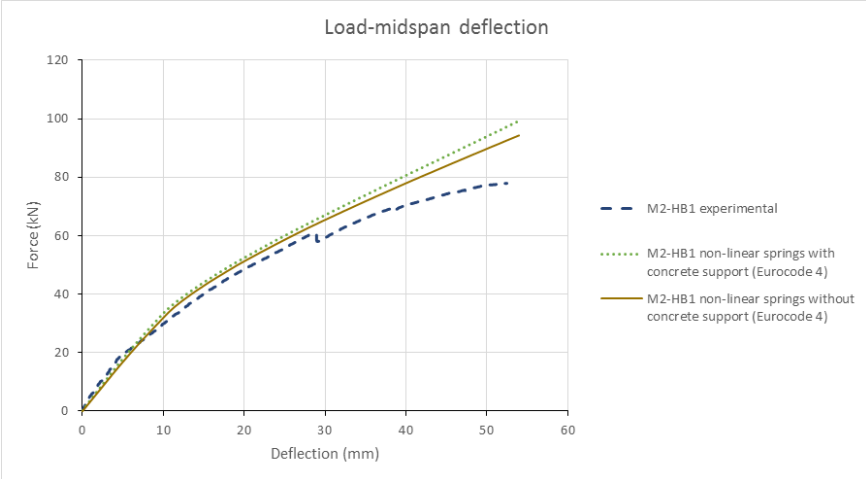

Figure 48. Load-midspan deflection comparative chart of the effect of the concrete reinforcement of the supports for M2-HB1 test

2.2. Refining the behaviour of concrete

Finally, the material model for concrete is refined, including the differences between compression and tension, and the softening when the crushing caused by excessive compressive loads appear. During the following sections, the different alternatives will be studied and its viability and complexity analysed, in order to finally choose the option which suits the most.

2.2.1. Multilinear elastic model

As a first option, a multilinear elastic model (MELAS) is studied. This model is a legacy model from Mechanical APDL, and it is not directly accessible from Workbench, so commands are necessary. This material model is defined as follows.

> *"The multilinear elasticity option (TB, MELAS) causes unloading to occur along the same path as loading. This behaviour, unlike other options, is conservative (path-independent). The plastic strain for this option should be interpreted as a "pseudo plastic strain" since it returns to zero when the material is unloaded (no hysteresis)."* (ANSYS Inc. 2013)

However, this model doesn't accept a different definition of the behaviour between tension and compression, so it wouldn't make any difference between the elastic-plastic models previously used, since the unloading of the beam is not a subject of interest of the present study. Moreover, the extra complexity of this option, which requires the use of commands (see Figure 49), makes this option not very suitable.

```
MP,EX,1,171746.988
MP,NUXY,1,0.3
TB,MISO,1,1,22
TBTEMP,0
TBPT,,0,0
TBPT,,0.00166,285.1
TBPT,,0.00207,285.14
TBPT,,0.00237,302.65
TBPT,,0.00266,320.19
TBPT,,0.00296,328.21
TBPT,,0.00355,336.35
TBPT,,0.00414,341.32
TBPT,,0.00473,343.12
TBPT,,0.00532,343.34
TBPT,,0.00591,343.55
TBPT,,0.00650,343.76
TBPT,,0.00709,343.98
TBPT,,0.00767,342.60
TBPT,,0.00826,341.21
TBPT,,0.00885,338.23
TBPT,,0.00944,327.27
TBPT,,0.01002,302.87
TBPT,,0.01032,268.45
TBPT,,0.01038,223.72
TBPT,,0.01038,191.76
TBPT,,0.01043,159.81
```

Figure 49. Example of a material model defined by the use of commands (XANSYS Forum 2012)

All these reasons, cause that finally, this alternative is discarded, and other possibilities are studied.

2.2.2. Hyperelastic models

Secondly, hyperelastic models are studied. These models are commonly used for rubbers and elastomers. However, there is a special hyperelastic model, called “response function”, which uses directly a series of experimental data points (from uniaxial, biaxial or shear tests) without using any specific hyperelastic model. Furthermore, hyperelastic models allow the user to introduce different properties for compression and for tension (see Figure 50). This model is recommended by ANSYS for users who want to define nonlinear elastic materials. However, this model is more complex, slow to solve and present some convergence difficulties, so at first hyperelastic models included in ANSYS will be used from simple to complex, and finally the response function model will be tested as well.

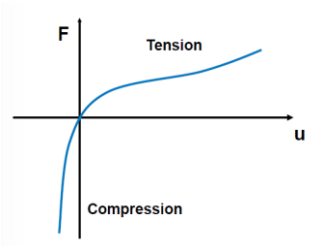

Figure 50. Example of the behaviour of an elastomer (hyperelastic model) (ANSYS Inc. 2012b)

In order to define correctly all the hyperelastic models, two types of experimental data are defined:

- Uniaxial test data
- Volumetric test data

On the one hand, in uniaxial test data stress-strain data points for concrete are introduced, without any softening at the beginning to enhance the convergence, as Figure 51 shows.

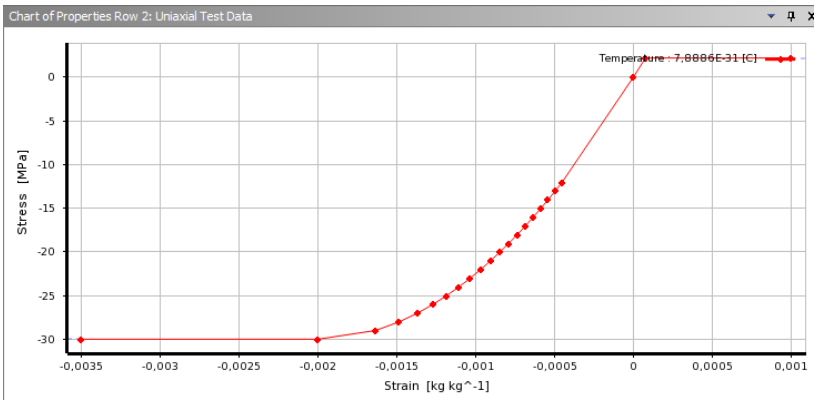

Figure 51. Chart for uniaxial test data of concrete (without softening)

On the other hand, volumetric test data is introduced in order to simulate the compressibility of the material (since the Poisson coefficient is not 0.5). This test data relates the hydrostatic pressure and the volume ratio. This relation is defined by the following equation.

$$P = k \cdot e_v \quad ; \quad k = \frac{E}{3(1-2v)}$$

Equation 2. Analytical formula that relates the hydrostatic pressure and the volume ratio

Using this information, in the following sections hyperelastic material models are used using the curve fitting option that ANSYS includes for hyperelastic models.

2.2.2.1. Neo-Hookean model

First of all, the simplest hyperelastic model is used. This model is not able to simulate the behaviour, in fact the difference between the uniaxial data and the model is very important, as Figure 52 shows.

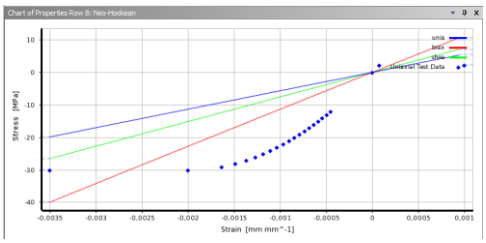

Figure 52. Comparative chart between the uniaxial test data and the Neo-Hookean model

Nevertheless, this first simulation is executed and converges without any problems (see Figure 53). Finally, Figure 54 presents the results of this model compared to the experimental tests and the previous definitive simulation with springs.

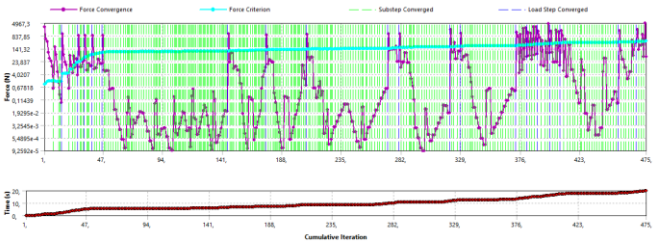

Figure 53. Force convergence chart for the Neo-Hookean simulation

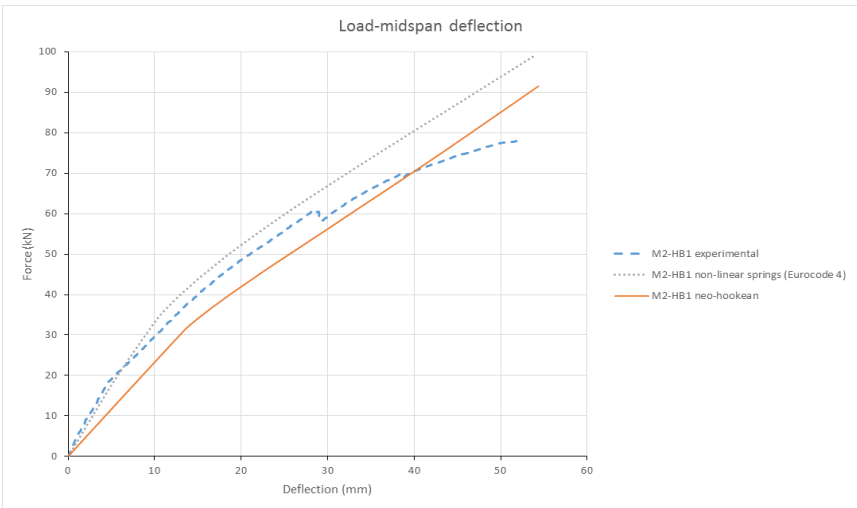

Figure 54. Load-midspan deflection results for M2-HB1 test using the Neo-Hookean hyperelastic model

Even though the results are not as bad as one could expect taking into account the differences between the material data and the model, this model is discarded because of its poor results.

2.2.2.2. Mooney-Rivilin 2 parameter

After the first approach using the Neo-Hookean model, a second approach is made using a Mooney-Rivilin 2 parameter model. This model, compared to the test data introduced is not as different, but it doesn't seem accurate enough for the problem (see Figure 55), since hyperelastic models are not thought for modelling concrete.

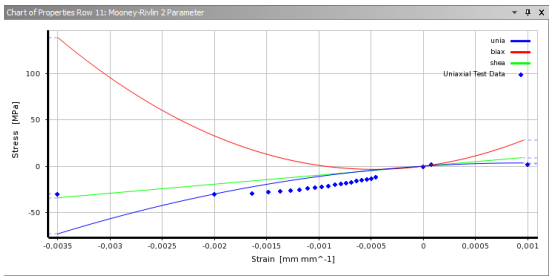

Figure 55. Comparative chart between the uniaxial test data and the Mooney-Rivilin 2 parameter model

Using this model convergence problems occur, as Figure 56 shows, and the solution fails after many bisections. However, the obtained results before the solution fails are presented in Figure 57.

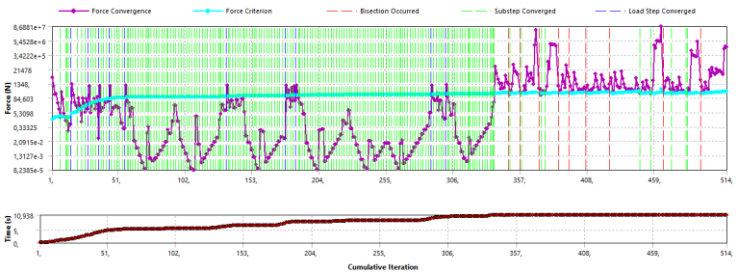

Figure 56. Force convergence chart for the Mooney-Rivilin 2 parameter simulation

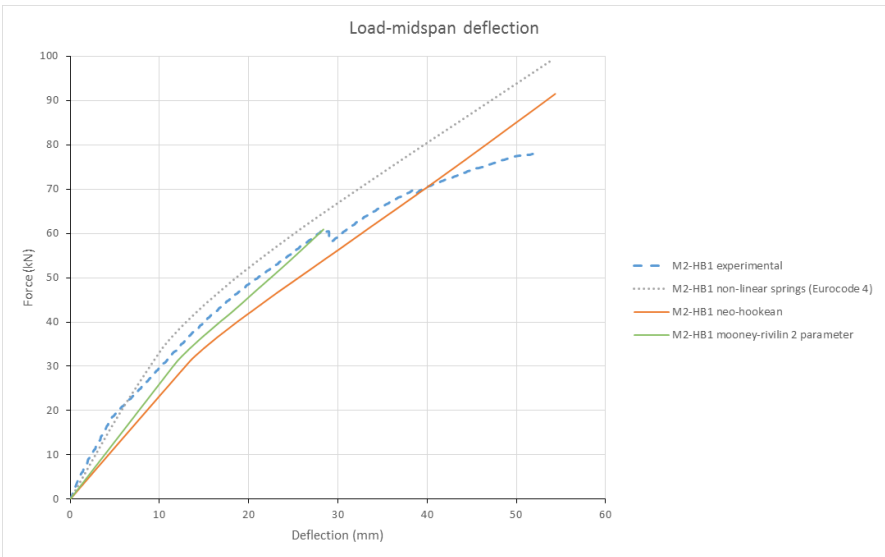

Figure 57. Load-midspan deflection results for M2-HB1 test using the Mooney-Rivilin 2 parameter hyperelastic model

In the previous chart it can be observed that compared to Neo-Hookean model, this one gives better results at the beginning. Nevertheless, it is not a good alternative, and it has many convergence difficulties, so it is discarded as well.

2.2.2.3. Response function

Finally, the response function model is used. As previously said, this model does not make any approximation from de data test in order to obtain a material constitutive law, it uses directly the data introduced in ANSYS. However, using this hyperelastic model many convergence problems appear, as can be observed in Figure 58. The solution fails without converging any step, even though the first one doesn't apply any displacement to the model. All these difficulties using hyperelastic models are the cause that these alternatives are discarded as well, in benefit of the option which is explained in the following section.

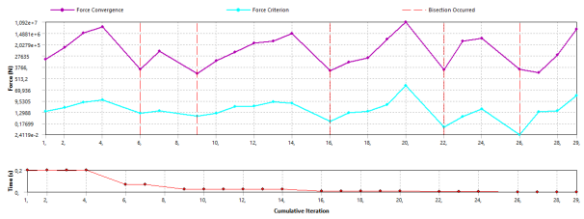

Figure 58. Force convergence chart for the response function simulation

2.2.3. Dividing the concrete in two different solids

Finally, the last alternative is studied. In this section, the simplicity of the beam and the loads are used to determine which parts of concrete are under compression and which under tension. If the concrete slab is divided by the neutral line, different properties can be defined for each solid and obtain a much more realistic model.

Figure 59 shows the distribution of normal stresses. Observing this distribution, one can observe that the concrete slab could be divided into an upper and a lower layer with different properties.

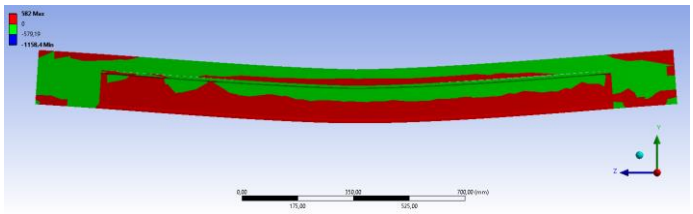

Figure 59. Distribution of compressive stresses (green) and tension stresses (red) of the beam

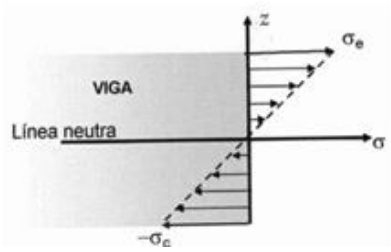

Figure 60. Schematic view of the stress distribution of the section, divided by the neutral line

In order to obtain good results using this alternative, the position of the neutral line is the most important parameter. The position of the neutral line, according to analytical analysis, is located at 30mm from the top of the concrete slab. However, in a first attempt to optimize this model, the line is positioned at the middle of the concrete slab.

2.2.3.1. Material models for the concrete slab

First of all, the material models are defined. In this case, the tension part will be included as well, so it is necessary to define it. In order to do so, a bilinear isotropic hardening plasticity model is used, using the ultimate tensile strength as the yield stress, as Figure 61 shows.

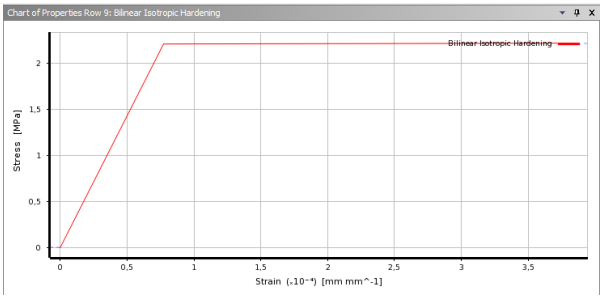

Figure 61. Bilinear isotropic hardening behaviour for concrete in tension

2.2.3.2. Optimization of the model

During the first approach, the same definitive model with springs is used, dividing the concrete slab in two layers, as Figure 62 shows. However, in this geometry, both layers are defined with its own material properties, depending on its position.

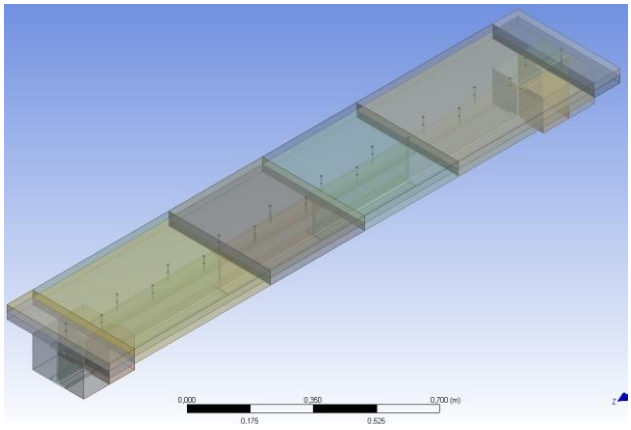

Figure 62. View of the compression and tension parts of the concrete slab geometry

In a very beginning, the springs are connecting the GFRP with the lower layer of the concrete slab (tension). However, with this formulation, the solution of the model fails after few steps converged. If the results are analysed, the conclusion obtained is that since the springs are not connected to the resistant part of the slab (the compression part), excessive deformations appear when the stresses reach 2.21MPa (ultimate tensile strength). The plastic strain results are especially significant, as can be observed in Figure 63.

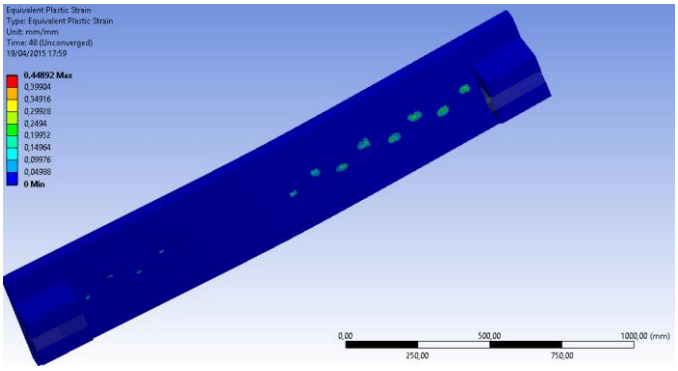

Figure 63. View of the excessive strains near the spring connectors

This problem is solved connecting the springs to the compressive part of the concrete slab, as can be observed in Figure 64, which shows one of the spring connectors. It can be appreciated on the image that between the highlighted solids there is the tension layer of the slab.

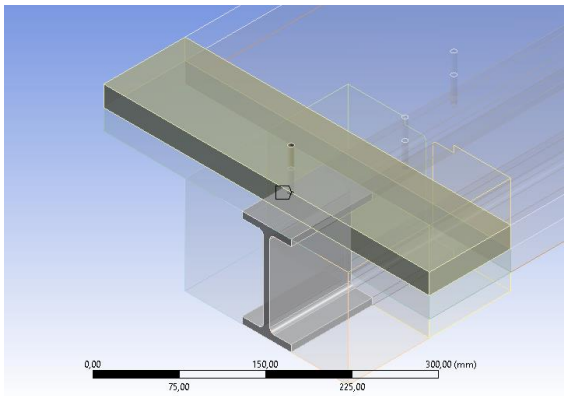

Figure 64. View of the spring connectors between GFRP and the compressive layer of the concrete slab

The figure below shows the initial results for M2-HB1 model. However, before performing the simulations for the rest of the tests, a parametric study of the position of the neutral line is made, in order to improve the model.

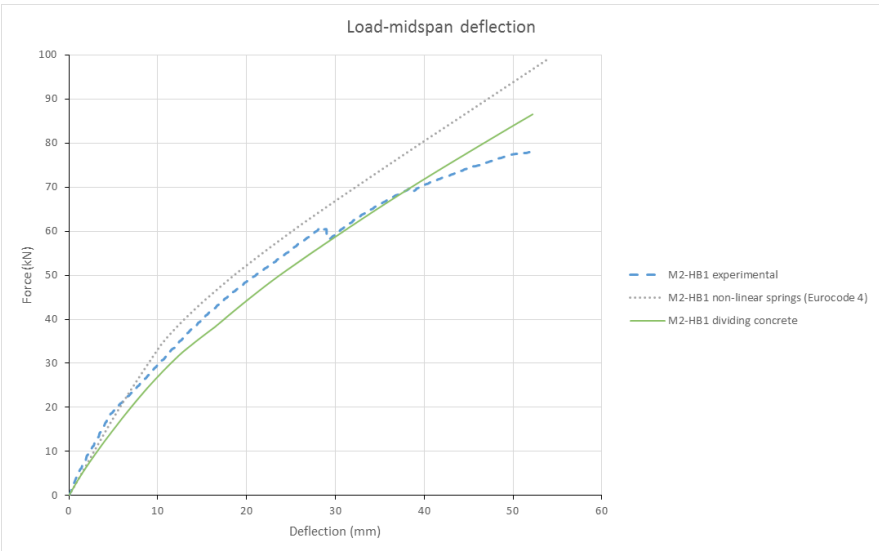

Figure 65. Load-midspan deflection initial results for M2-HB1 dividing concrete in two parts

2.2.3.3. Parametric study of the position of the neutral line

In order to do this study, the response surface component from Design Exploration is used. The position of the neutral line is the input parameter, and the total applied force (only the maximum value) is the output parameter, as can be observed in the figure below.

Outline of All Parameters

	A	B	C	D
1	ID	Parameter Name	Value	Unit
2	Input Parameters			
3	M2-HB1 plasticity millorat (A1)			
4	P1	Plane4.FD1	85	mm
*	New input parameter	New name	New expression	
6	Output Parameters			
7	M2-HB1 plasticity millorat (A1)			
8	P2	Force Reaction Total	86553	N
*	New output parameter		New expression	
10	Charts			

Figure 66. Input and output parameters used in the response surface component

The response surface component will generate a mathematical model that will approximate the obtained force reaction total (output) as a function of the position of the neutral line (input). In order to fit the resultant curve with the experimental data, the desired output should be around 90-92kN.

Figure 67 shows the introduced range of study for the position of the neutral line. After this, ANSYS will make a series of simulations and will create the mathematical model previously said.

Properties of Outline A5: P1 - Plane4.FD1

	A	B
1	Property	Value
2	General	
3	Units	mm
4	Type	Design Variable
5	Classification	Continuous
6	Values	
7	Value	85
8	Lower Bound	65
9	Upper Bound	90
10	Use Manufacturable Values	

Figure 67. Configuration for the input parameter in the response surface component

The design points that have been created and simulated, in order to generate the mathematical model are presented in Figure 68.

Table of Schematic B2: Design of Experiments (Central Composite Design : Auto Defined)

	A	B	C	D
1	Name	Update Order	P1 - Plane4.FD1 (mm)	P2 - Force Reaction Total (N)
2	1 (DP 3)	3	77,5	
3	2	1	65	97981
4	3	5	90	83492
5	4	2	71,25	93248
6	5 (DP 4)	4	83,75	

Figure 68. Design points automatically generated and its results

As can be observed, two of the five points have failed during the solution, so they don't have results. However, the correlation and the tendency of the three obtained solutions are studied. Since their regression, as Figure 69 shows, is very accurate, using this correlation the optimum position of the neutral line is determined.

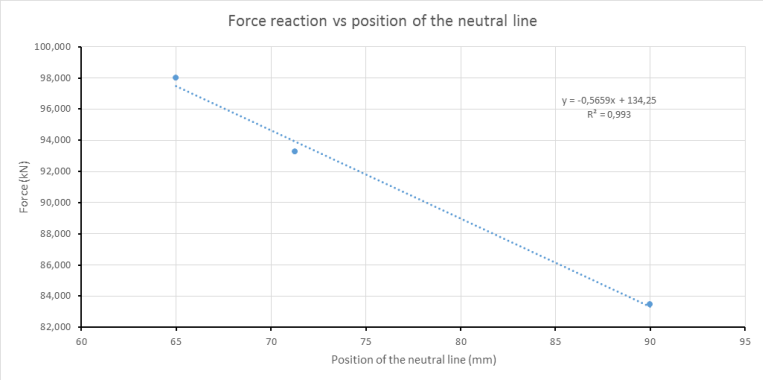

Figure 69. Force vs position of the neutral line chart

In order to determine the position of the neutral line, first of all the deflection and the force at which crushing occurs (softening of concrete starts) during the experiment are determined. With these values, compared to the force for the definitive model with springs (Eurocode 4), the maximum value of the force for the experiment (without softening of the material) is extrapolated in order to introduce it in the correlation previously found, and determine the optimum position of the neutral line.

Table 2. Extrapolation of the maximum force of the beam M2-HB1 without softening of concrete

	Experimental data	**Model with springs (Eurocode 4)**
Deflection when crushing occurs (mm)	28,521	28,521
Force when crushing occurs (kN)	60,36	64,876
Maximum force (without softening) (kN)	92,2	99,105

In order to clarify the different points that have been used for the extrapolation, the following figure shows a more detailed view. The point when crushing occurs is the orange one, and the point of maximum force (without softening of the material) can be observed in red.

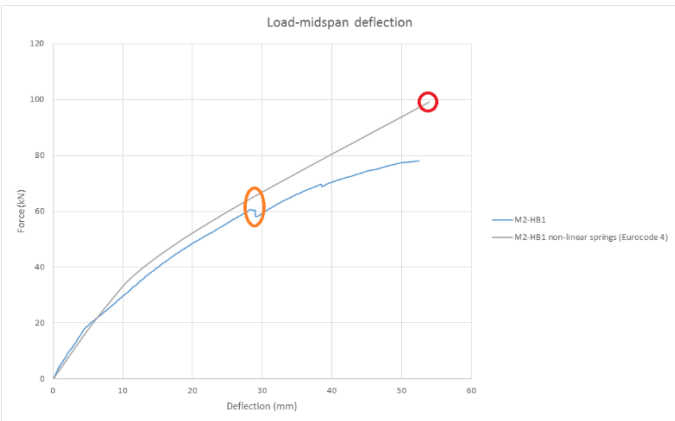

Figure 70. Detailed view of the result points used for the extrapolation

Introducing the obtained maximum force in the mathematical equation previously obtained, the optimum position of the neutral line is obtained.

$$F = 134.25 - 0.5659X = 92.2\ kN \rightarrow X = 74.3mm$$

Equation 3. Determination of the optimum position of the neutral line

The optimum value is then a compressive layer of 35.7 mm of thickness and a tension layer of 14.3 mm of thickness. These values are slightly different from the theoretical ones (30mm and

20mm respectively). Using this values a new simulation is executed, so the results can be checked.

2.2.3.4. Final results with the definitive model

Finally, the definitive model is executed for all the tests. The first figure, shows the results for M2-HB1 test. It can be observed that the previous predictions and estimations were correct, since the model fits very well the experimental test (the maximum force is 91.6kN, very close to the predicted in the previous section). Moreover, the model is good as well for the rest of the test, with its own materials and loading schemes.

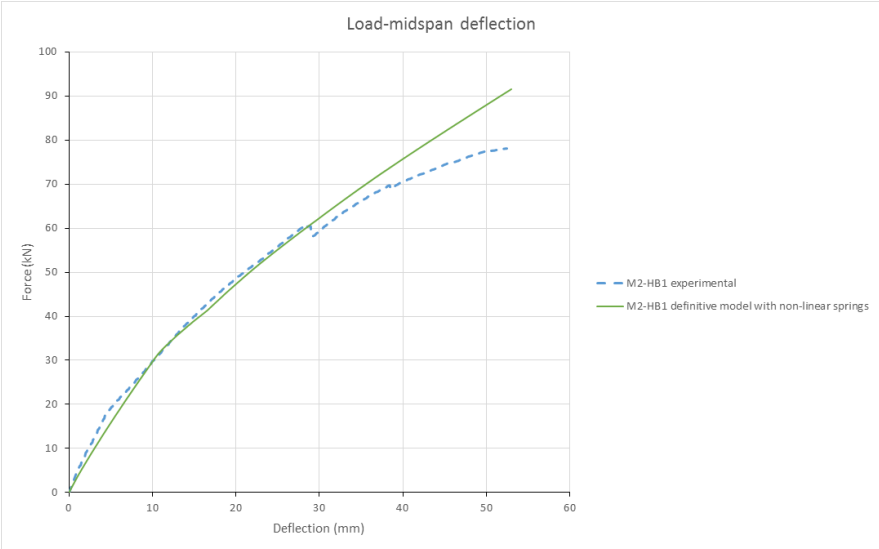

Figure 71. Load-midspan deflection results for M2-HB1 of the definitive model

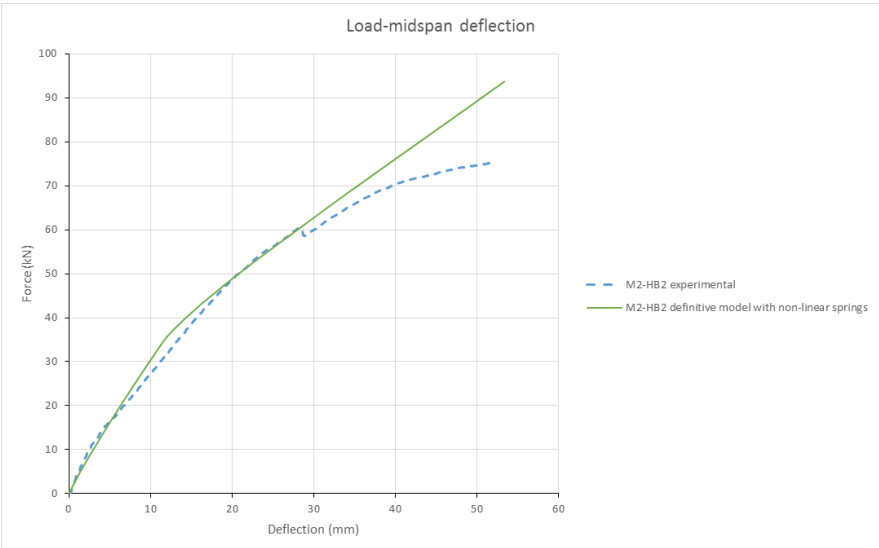

Figure 72. Load-midspan deflection results for M2-HB2 of the definitive model

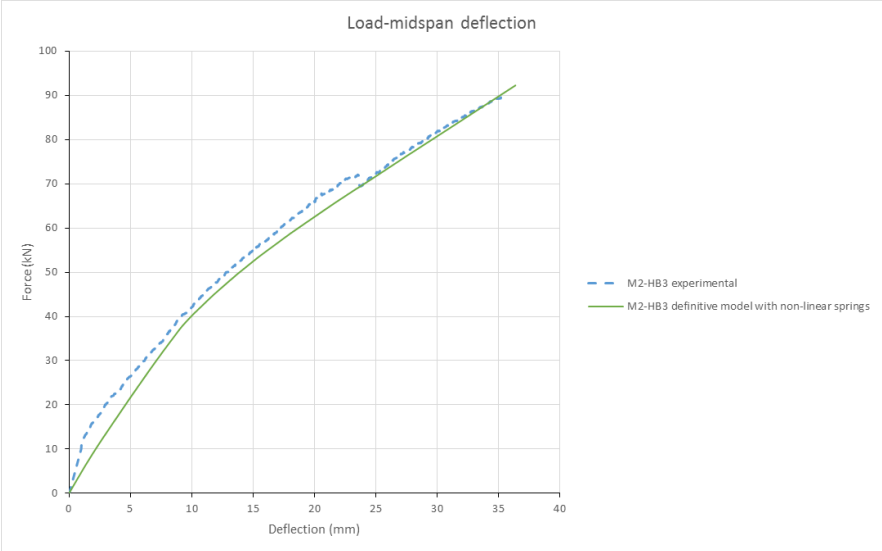

Figure 73. Load-midspan deflection results for M2-HB3 of the definitive model

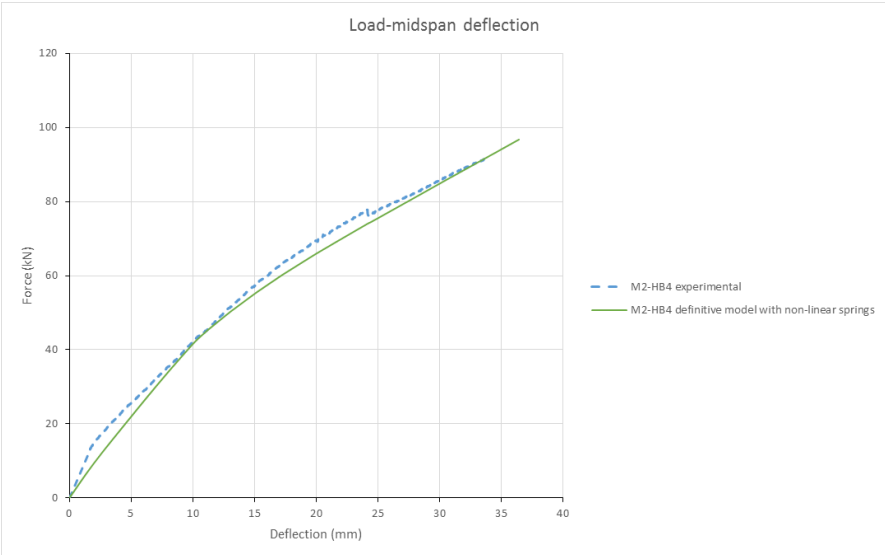

Figure 74. Load-midspan deflection results for M2-HB4 of the definitive model

References

ANSYS, 2010. Introduction to Contact ANSYS Mechanical Structural Nonlinearities.

ANSYS Inc., 2012a. ANSYS Mechanical APDL Element Reference. *ANSYS Manual*, 15317(November), pp.1377–1390.

ANSYS Inc., 2013. ANSYS Mechanical APDL Feature Archive. , 15317(November), pp.724–746.

ANSYS Inc., 2012b. Hyperelasticity ANSYS Mechanical Advanced Nonlinear Materials. , pp.2011–2013.

European Standard, 2004. Eurocode 4 : Design of composite steel and concrete structures Part 1-1 : General rules and rules for buildings. , pp.1–117.

International Federation for Structural Concrete, 2010. *Model Code*,

XANSYS Forum, 2012. Using commands to introduce a material model. Available at: http://xansys.org/forum/viewtopic.php?p=88418 [Accessed April 16, 2015].